Position Control of a Sensorless Stepper Motor

Moussa Bendjedia, Youcef Ait Amirat, Bernard Walther, Alain Berthon

Position Control of a Sensorless Stepper Motor

Moussa Bendjedia, Youcef Ait-Amirat, *Member, IEEE*, Bernard Walther, and Alain Berthon, *Member, IEEE*

***Abstract*—In this paper, the experimental results of position control of the hybrid stepper motor without a mechanical sensor are exhibited. Use of the steady-state extended Kalman filter to estimate the mechanical variables of the motor is shown. With this method the computing time is reduced. The initial rotor position is estimated by the impulse voltage technique. For position control, a simple state feedback control that can compensate the load torque variations was designed. The robustness against the motor parameters variation was also studied. A field-oriented control strategy is chosen. It is known that the mechanical position is crucially important to achieve this strategy. Finally, favorable experimental results are shared.**

***Index Terms*—DSP, extended Kalman filter (EKF), feedback control, field-oriented control, hybrid stepper motor (HSM), position control, sensorless.**

I. Introduction

THE HYBRID stepper motor [1] is used in several industrial applications where torque at low speed, positioning accuracy, and high-speed dynamic are determining factors. It can, thus, be found in numerous applications. For example in medical applications for, accurate dosage with peristaltic pumps or pipettes and motion control in dialysis equipment. Also, in automotive applications, combustion engines contain several systems to control emissions and reduce NO_x level. These systems always combine a stepper motor that drives efficiently integrated valves. In telecommunications, the stepper motor is used to actuate antennas and combiners. All these applications require a robust actuator that can withstand vibrations and must respond quickly and precisely to a signal position, while at the same time guaranteeing that it can overcome a dynamic torque load.

The stepper motor has the advantage over other kinds of motors because it works well in open loop since it carries out motion step by step when voltage impulses are applied to its phases. But, due to its inertia, the rotor oscillates around the final position before stabilizing. In addition, the motor can lose steps if the variation of the load torque is fast. The use of new programmable architecture like field-programmable gate arrays (FPGA) circuit [2] allows the creation of microstep movements. That smoothes the movement but leaves the open-loop control problem unsolved. To solve it, it is necessary to introduce a closed loop to improve the performance and the robustness of the control. A first solution was the introduction of mechanical sensors. This solution increases the size and the cost of the system. Furthermore, analysis of past experience from automotive applications, for example, shows that mechanical measures such as position or speed suffer in high-temperature- and high-vibration environment. Due to these limitations, sensorless control emerges, with today's low cost and high-performance DSP's, as an alternative and a very interesting solution since it saves the expensive and bulky mechanical sensor.

Several sensorless methods including standstill were proposed for various motors and can be applied to the stepper motor. The knowledge of the initial rotor position guarantees a starting of the motor in the desired direction [3]. The standstill methods [4], [5] are based on the inductance variation according to the rotor position. Voltage signals are injected to the windings and the initial rotor position is obtained by monitoring the phase currents. For low speed, this principle is used in [6] to estimate the rotor position without voltage injection. The phase incremental inductance is estimated in real time and compared to an analytical model to estimate the rotor position. The high-frequency signal injection method [7]–[10] can detect the initial rotor position and extend the estimation to low speeds. The back electromotive force method is widely used because of its easy implementation [11]–[16]. For middle and high speeds, the observers are more suitable. The sliding mode observer is characterized by its robustness against the disturbance and motor parameters variation as shown in [17] and [18]. A new nonlinear observer has been recently proposed in [19] to estimate the rotor position without information about the motor speed. The extended Kalman filter (EKF) [20] is often used in the speed sensorless control because it has low-pass filter characteristics. To reduce the computing time of the EKF algorithm, [21] assumed an infinite inertia of the motor. Unscented Kalman filter [22] can improve the estimate and reduce the computing time. In [23], use of the Kalman filter in steady-state case for hybrid stepper motor with a speed control is proposed, but only simulation results were shown. The position control of the stepper motor is the subject of many pieces of research [24] that integrates a mechanical sensor.

This study proposes to investigate a simplified version of the EKF algorithm to estimate the mechanical state variables of the stepper motor by only measuring the line voltages and currents. Then, the feedback control is achieved from these estimated variables instead of the measured ones. Furthermore, by applying the principle of field orientation, the dynamic performance of the stepper motor is considerably improved

M. Bendjedia is with the Laboratoire des Sciences de l'Information et des Systèmes, Ecole Centrale Marseille, Marseille 13397, France (e-mail: moussa.bendjedia@centrale-marseille.fr).

Y. Ait-Amirat is with the University of Franche-Comté, Besançon 25000, France (e-mail: youcef.ait-amirat@univ-fcomte.fr).

B. Walther is with the Haute Ecole Arc Engineering, Saint-Imier CH-2610, Switzerland (e-mail: bernard.walther@he-arc.ch).

A. Berthon is with the University of Franche-Comté, Belfort 90010, France (e-mail: alain.berthon@univ-fcomte.fr).

and it becomes a high-dynamic ac drive. We also discuss the robustness of the approach. The stepper motor has a low power, quite small electrical parameter, and high pair number of pole pairs compared to other sensorless research. Thus, great care was taken in the design of the electronic card made for this paper. For example, the phase voltages and currents are well filtered by this card before being acquired by the dSPACE DS1103.

II. Motor Model and EKF Basics

The hybrid stepper motor (HSM) is a synchronous motor with two phases *A* and *B* in quadrature; therefore, mutual inductances are null. So the motor can be represented by the following electric equations

$$\begin{aligned} u_a &= Ri_a + L\frac{di_a}{dt} - K_m\omega\sin(N\theta) \\ u_b &= Ri_b + L\frac{di_b}{dt} - K_m\omega\cos(N\theta) \end{aligned} \tag{1}$$

where i_a and i_b are the currents of phases *A* and *B* (A), u_a and u_b are the phase voltages (V), *R* is the phase resistance (Ω), *L* is the phase inductance (H), K_m is the torque constant (V·s/rad), ω is the angular velocity (rad/s), θ is the mechanical rotor position (rad), and *N* is the rotor number teeth.

The mechanical equations of the HSM can be written in the following form

$$\begin{aligned} K_m(-i_a\sin(N\theta) + i_b\cos(N\theta) - T_L &= J\frac{d\omega}{dt} + K_v\omega \\ \omega &= \frac{d\theta}{dt} \end{aligned} \tag{2}$$

where K_v is the coefficient of viscous friction (N·m·s/rad), *J* is the system inertia (kg·m^2), and T_L is the load torque (N·m).

Applying the Park transformation to (1) and (2), the model of the HSM in the rotating frame (*d*,*q*) becomes

$$\begin{cases} u_d = Ri_d + L\dfrac{di_d}{dt} - LN\omega i_q \\ u_q = Ri_q + L\dfrac{di_q}{dt} + LN\omega i_d + K_m\omega \\ K_m i_q - T_L = J\dfrac{d\omega}{dt} + K_v\omega \\ \dfrac{d\theta}{dt} = \omega. \end{cases} \tag{3}$$

We carried out practical tests to properly identify the model parameters which are: $R = 0.37$ (Ω), $L = 0.9$ (mH), $K_m = 0.157$ (V·s/rad), $K_v = 0.000307$ (N·m·s/rad), $J = 15.62 \times 10^{-5}$ (Kg·m^2), and $N = 50$.

The field-oriented control method is used to control the flux and the torque of the motor independently. The *d*-axis is chosen on the flux axis, so all the flux is aligned along this axis. The torque is managed by controlling the current in the *q*-axis. However, there are coupling items in current equations (3). In order to have linear and decoupling terms, the *d*–*q* axis stator voltage (3) can be expressed in two components

$$\begin{aligned} u_d &= u_d^{\text{lin}} + u_d^{\text{dec}} = \left(Ri_d + L\frac{di_d}{dt}\right) - LN\omega i_q \\ u_q &= u_q^{\text{lin}} + u_q^{\text{dec}} = \left(Ri_q + L\frac{di_q}{dt}\right) + LN\omega i_d + K_m\omega \end{aligned} \tag{4}$$

where the *d*–*q* axis linear voltage components are

$$u_d^{\text{lin}} = Ri_d + L\frac{di_d}{dt} \text{ and } u_q^{\text{lin}} = Ri_q + L\frac{di_q}{dt}. \tag{5}$$

And the *d*–*q* axis decoupling voltage components are

$$u_d^{\text{dec}} = -LN\omega i_q \text{ and } u_q^{\text{dec}} = LN\omega i_d + K_m\omega. \tag{6}$$

The linear voltage components V_d^{lin}, V_q^{lin} are the outputs of the current controllers and are added to the decoupling voltage components u_d^{dec} and u_q^{dec}.

The EKF was proposed for the nonlinear systems as in (3). It uses the discrete system model in the following state space form

$$\begin{cases} \underline{x}_{k+1} = \underline{x}_k + T\cdot\underline{f}(\underline{x}_k, \underline{u}_k) + \underline{w}_k \\ \underline{y}_k = \underline{h}(\underline{x}_k) + \underline{v}_k \end{cases} \tag{7}$$

with $\underline{x}_k = [i_{dk} \quad i_{qk} \quad \omega_{dk} \quad \theta_{dk} \quad T_{Lk}]^{\text{t}}$ being the state vector, $\underline{u}_k = [u_{dk} \quad u_{qk}]^t$ being the input vector, and $\underline{y}_k = [i_{dk} \quad i_{qk}]^t$ being the output vector.

A suitable choice of the sampling period ($T = 100$ μs) is done with regard to system electric constant. The load torque is estimated by introducing it as a state variable. It is assumed that it is a perturbation and does not vary since the sampling period *T* is very small. The vector $\underline{w}_k$ represents the noise due to the errors of system modeling. The vector $\underline{v}_k$ represents the measurement noise. $\underline{w}_k$ and $\underline{v}_k$ are presumed to be zero-mean white Gaussian noises with covariance matrices $\boldsymbol{Q}k$ and $\boldsymbol{R}k$, respectively.

The EKF algorithm contains five equations and two phases.

1) The Prediction phase is

$$\underline{\hat{x}}_{k+1/k} = \underline{\hat{x}}_{k/k} + T\underline{f}(\underline{\hat{x}}_{k/k}, \underline{u}_k) \tag{8}$$

$$\boldsymbol{P}_{k+1/k} = \boldsymbol{F}\boldsymbol{d}_k\boldsymbol{P}_{k/k}\boldsymbol{F}\boldsymbol{d}_k^t + \boldsymbol{Q}_k \tag{9}$$

$$\boldsymbol{K}_{k+1} = \boldsymbol{P}_{k+1/k}\boldsymbol{H}_k^t\left(\boldsymbol{H}_k\boldsymbol{P}_{k+1/k}\boldsymbol{H}_k^t + \boldsymbol{R}_k\right)^{-1} \tag{10}$$

2) The Correction phase is

$$\underline{\hat{x}}_{k+1/k+1} = \underline{\hat{x}}_{k+1/k} + \boldsymbol{K}_{k+1}(\underline{y}_{k+1} - \boldsymbol{H}_k\underline{\hat{x}}_{k+1/k}) \tag{11}$$

$$\boldsymbol{P}_{k+1/k+1} = \boldsymbol{P}_{k+1/k} - \boldsymbol{K}_{k+1}\boldsymbol{H}_k\boldsymbol{P}_{k+1/k} \tag{12}$$

where $\boldsymbol{K}$ is the Kalman gain matrix, $\boldsymbol{P}$ is the covariance matrix, $\boldsymbol{Fd}$ is the Jacobian matrix of the system, and $\boldsymbol{H}$ is the Jacobian matrix of the output.

In the case of the steady-state EKF, the gain matrix $\boldsymbol{K}$ is computed offline. To do that, a simulation of the whole system was carried out with the complete EKF (8)–(12) while trying to use the same conditions of the real system which are the same sampling period, a good identification of the motor parameters, modeling the power converter, and adding some noises to the inputs of the EKF algorithm.

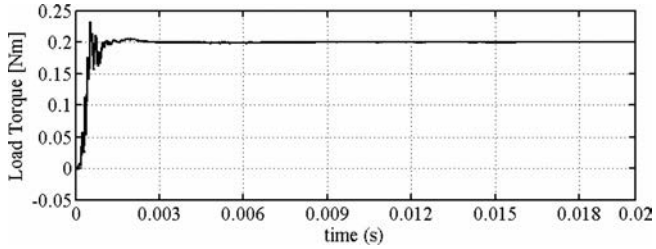

Fig. 1. Estimated load torque with $P_0(5, 5) = 50$.

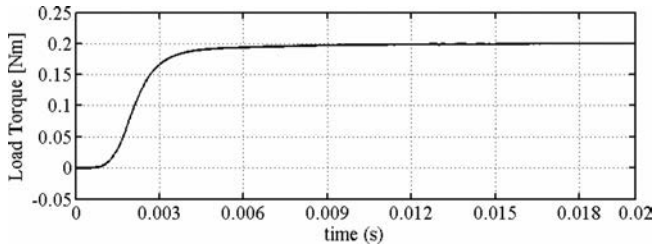

Fig. 2. Estimated load torque with $P_0(5, 5) = 0.02$.

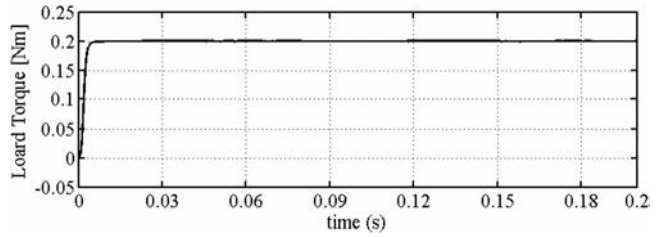

Fig. 3. Estimated load torque with $R = 100$.

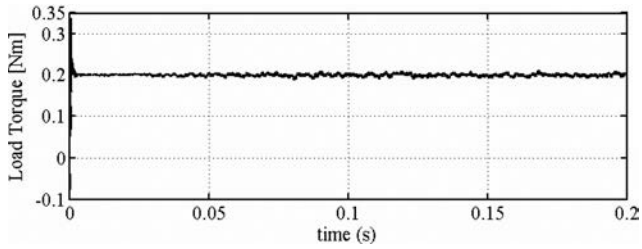

Fig. 4. Estimated load torque with $R = 0.001$.

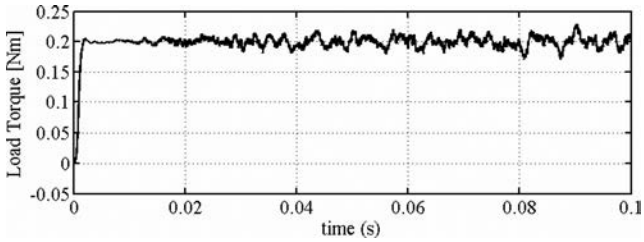

Fig. 5. Estimated load torque with $Q(5, 5) = 0.001$.

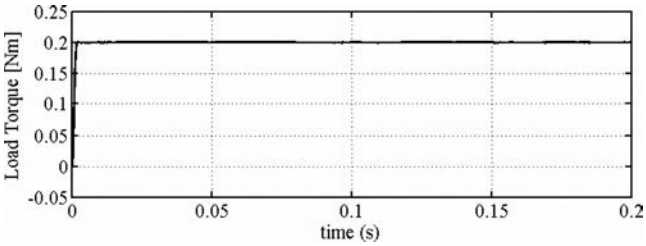

Fig. 6. Estimated load torque with $Q(5, 5) = 10^{-9}$.

A good estimation of the state variables is dependent upon the initial covariance matrices ($\boldsymbol{P}_0$, $\boldsymbol{R}$, and $\boldsymbol{Q}$) that are chosen. A recent work [25] tries to exhibit an algorithm called evolutionary algorithm to optimize the choice of these matrices. It is an iterative algorithm inspired by genetic algorithms and is based on numerous simulations. In this paper, these matrices are obtained after several simulation tests. A slight change is made on the value of a matrix and then its influence on the corresponding state variable is examined. For example, the value $\boldsymbol{P}_0(5,5)$ acts on the estimation of the load torque T_L. A large value of $\boldsymbol{P}_0(5,5)$ leads to faster transient response (see Fig. 1). We can observe in (10) that the Kalman gain matrix $\boldsymbol{K}$ is proportional to the matrix $\boldsymbol{P}$, so a large value in $\boldsymbol{P}$ leads to a large value of $\boldsymbol{K}$ and then the correction on the estimation variable becomes faster with possible apparition of overshoot. Otherwise, a large transient response is obtained (see Fig. 2). But, in both cases, the steady state of the estimated load torque is not affected.

The covariance matrix $\boldsymbol{R}$ represents the noises on the measure due to imperfections of the current and/or voltage sensors. If large values of matrix $\boldsymbol{R}$ are used, the transient response increases but the load torque is well estimated in steady state (see Fig. 3). As shown in (10), the matrices $\boldsymbol{K}$ and $\boldsymbol{R}$ are inversely proportional. So the values of $\boldsymbol{K}$ become weak in order to give more accuracy to the estimation of the load torque. Otherwise, overshoot in the transient response and noises in the steady-state response are obtained (see Fig. 4). In both cases, $\boldsymbol{R}$ acts on the transient response and in the steady-state response because its value is constant in the EKE algorithm.

The covariance matrix $\boldsymbol{Q}$ represents the noises on the system due to the modeling errors. The simulation results in Figs. 5 and 6 show the influence of this matrix on the estimation of the load torque. From (9) and (10), we notice that the matrix $\boldsymbol{K}$ is proportional to matrix $\boldsymbol{Q}$. Then, it has an opposite effect of that of $\boldsymbol{R}$. But matrix $\boldsymbol{Q}$ has no effect in the transient response because the covariance matrix $\boldsymbol{P}$ computed by (9) is dominated by the initial value of $\boldsymbol{P}_0$.

The choice of every value of these matrices is done according to the dynamics of the associated state variable. On the other hand, we notice that if the noises on the measure are weak and the model of the system is better known, the EKF algorithm becomes more precise. Good simulation results with the following matrices

$$\boldsymbol{P}_0 = \begin{bmatrix} 10^{-4} & 0 & 0 & 0 & 0 \\ 0 & 10^{-4} & 0 & 0 & 0 \\ 0 & 0 & 100 & 0 & 0 \\ 0 & 0 & 0 & 1 & 0 \\ 0 & 0 & 0 & 0 & 1 \end{bmatrix}$$

$$\boldsymbol{Q} = \begin{bmatrix} 10^{-4} & 0 & 0 & 0 & 0 \\ 0 & 10^{-4} & 0 & 0 & 0 \\ 0 & 0 & 10^{-3} & 0 & 0 \\ 0 & 0 & 0 & 10^{-6} & 0 \\ 0 & 0 & 0 & 0 & 10^{-6} \end{bmatrix} \boldsymbol{R} = \begin{bmatrix} 1 & 0 \\ 0 & 1 \end{bmatrix}.$$

For the implementation in real time, we used only two equations (8) and (11) with a matrix gain $\boldsymbol{K}$ constant obtained by simulation. As a result, the computing time is drastically reduced.

III. Position Control

The stepper motor is generally used in position control where good precision is required. In this paper, a simple feedback control was used. The rotor position is not measured by a mechanical sensor but estimated by the steady-state EKF presented in Section II.

A. Discrete Model in State Space

The discrete model in state space is needed to determine the control laws of the feedback control. The mechanical equations of the model (3) can be written as

$$\begin{bmatrix} \dot{\omega} \\ \dot{\theta} \end{bmatrix} = \begin{bmatrix} -\frac{K_v}{J} & 0 \\ 1 & 0 \end{bmatrix} \begin{bmatrix} \omega \\ \theta \end{bmatrix} + \begin{bmatrix} \frac{K_m}{J} \\ 0 \end{bmatrix} I_q + \begin{bmatrix} -\frac{1}{J} \\ 0 \end{bmatrix} T_L. \tag{13}$$

We can write (13) in the following form

$$\underline{\dot{x}_m} = \boldsymbol{A_m}\underline{x_m} + \boldsymbol{B_m}\, I_q + \boldsymbol{E_m} T_L \tag{14}$$

with

$$\underline{x_m} = \begin{bmatrix} \omega \\ \theta \end{bmatrix}, \boldsymbol{A_m} = \begin{bmatrix} -\frac{K_v}{J} & 0 \\ 1 & 0 \end{bmatrix}, \boldsymbol{B_m} = \begin{bmatrix} \frac{K_m}{J} \\ 0 \end{bmatrix},$$

and $\boldsymbol{E_m} = \begin{bmatrix} -\frac{1}{J} \\ 0 \end{bmatrix}$.

Applying the Laplace transform to (14), we obtain

$$\underline{X_m}(p) = \boldsymbol{\Phi}(p)\underline{x_m}(0) + \boldsymbol{\Phi}(p)\boldsymbol{B_m}\, I_q(p) + \boldsymbol{\Phi}(p)\boldsymbol{E_m} T_L(p) \tag{15}$$

with $\boldsymbol{\Phi}(p) = [p\boldsymbol{I} - \boldsymbol{A_m}]^{-1}$, p being the Laplace operator, and I being the identity matrix.

Applying the inverse Laplace transform and the convolution theorem, we find the temporal response of (15) as

$$\underline{x_m}(t) = \boldsymbol{\Phi}(t-t_0)\underline{x_m}(t_0) + \int_{t_0}^{t} \boldsymbol{\Phi}(t-\tau) B_m\, I_q(\tau) d\tau + \int_{t_0}^{t} \boldsymbol{\Phi}(t-\tau) E_m T_L(\tau) d\tau. \tag{16}$$

To have the discrete form, it is enough to replace $t_0 = kT$ and $t = kT + T$. If we assume that the system inputs I_q and T_L do not change during the sampling period T, we obtain

$$\underline{x_m}(kT+T) = \boldsymbol{\Phi}(T)\underline{x_m}(kT) + \int_{kT}^{kT+T} \boldsymbol{\Phi}(kT+T-\tau) B_m\, I_q(kT) d\tau + \int_{kT}^{kT+T} \boldsymbol{\Phi}(kT+T-\tau) E_m T_L(kT) d\tau. \tag{17}$$

After the development of (17), we find the state representation of the system

$$\begin{cases} \underline{x_m}(k+1) = \boldsymbol{A_{mk}}\underline{x_m}(k) + \boldsymbol{B_{mk}}\, I_q(k) + \boldsymbol{E_{mk}} T_L(k) \\ \underline{y_m}(k) = \theta(k) = [\,0 \quad 1\,]\,\underline{x_m}(k) \end{cases} \tag{18}$$

with

$$\boldsymbol{A}_{mk} = \begin{bmatrix} a_{11k} & 0 \\ a_{21k} & 1 \end{bmatrix}; \boldsymbol{B}_{mk} = \begin{bmatrix} b_{1k} \\ b_{2k} \end{bmatrix}; \boldsymbol{E}_{mk} = \begin{bmatrix} e_{1k} \\ e_{2k} \end{bmatrix};$$

$$a_{11k} = e^{-\frac{K_v}{J}T}; a_{21k} = \frac{J}{K_v}\left(1 - e^{-\frac{K_v}{J}T}\right);$$

$$b_{1k} = \frac{K_m}{K_v}\left(1 - e^{-\frac{K_v}{J}T}\right); b_{2k} = \frac{K_m}{K_v}\left(T - \frac{J}{K_v}\left(1 - e^{-\frac{K_v}{J}T}\right)\right);$$

$$e_{1k} = -\frac{1}{K_v}\left(1 - e^{-\frac{K_v}{J}T}\right); e_{2k} = -\frac{1}{K_v}\left(T - \frac{J}{K_v}\left(1 - e^{-\frac{K_v}{J}T}\right)\right).$$

B. Feedback Controller Synthesis

In the state feedback controller, the current reference I_q^* is computed according to the estimated state variables ($\hat{\theta}$ and $\hat{\omega}$). A direct intervention of the reference position and another one to compensate the load torque are added. The feedback controller is represented by the following equation

$$I_q^*(k) = -K_\omega \hat{\omega}(k) - K_\theta \hat{\theta}(k) + K_{\theta^*}\theta^*(k) + K_L \hat{T}_L(k). \tag{19}$$

The coefficients K_ω and K_θ are computed by imposing poles in closed-loop system using a canonical form method. The characteristic equation in the open loop of the model (18) is given by

$$\det(z\boldsymbol{I} - \boldsymbol{A}_{mk}) = z^2 + \alpha_1 z + \alpha_0 \tag{20}$$

with $\alpha_0 = e^{-(K_v/J)T}$ and $\alpha_1 = -(e^{-(K_v/J)T} + 1)$.

The canonical form of the open-loop system is

$$\underline{x_r}(k+1) = \boldsymbol{A}_r\underline{x_r}(k) + \boldsymbol{B}_r I_q^*(k) \tag{21}$$

with $\boldsymbol{A}_r = \begin{bmatrix} 0 & 1 \\ -\alpha_0 & -\alpha_1 \end{bmatrix}$, $\boldsymbol{B}_r = \begin{bmatrix} 1 \\ 0 \end{bmatrix}$, and $\underline{x_r}$ is the state vector of the canonical form

$$I_q^*(k) = [K_{r\omega} \quad K_{r\theta}]\, x_r\,(k) \tag{22}$$

where $K_r\omega$ and $K_{r\theta}$ are the coefficients of the canonical form.

If we replace (22) in (21), we obtain the canonical form of the closed loop

$$\underline{x_r}(k+1) = \boldsymbol{A_f}\underline{x_r}(k) \tag{23}$$

with $\boldsymbol{A_f} = \begin{bmatrix} 0 & 1 \\ -(\alpha_0 + K_{r\omega}) & -(\alpha_1 + K_{r\theta}) \end{bmatrix}$.

To obtain the value of $K_r\omega$ and $K_{r\theta}$, the system (23) is compared with the reference model. The choice of the poles of this reference model is done according to the desired performances for the closed loop. Since we have a second-order system (3), we choose a double real pole, which makes it possible to avoid the overshoot. The characteristic equation of the reference model with a double real pole is given by

$$P(z) = z^2 + z_1 z + z_0 \tag{24}$$

with $z_1 = -2e^{-\omega_0 T}$, $z_0 = e^{-2\omega_0 T}$, and ω_0 is the pulsation.

The canonical form of (24) is

$$\boldsymbol{A_d} = \begin{bmatrix} 0 & 1 \\ -z_0 & -z_1 \end{bmatrix}. \tag{25}$$

The identification between the two matrices $\boldsymbol{A}_f$ (23) and $\boldsymbol{A}_d$ (25) makes it possible to find the state tuning coefficients of the canonical form

$$\begin{cases} K_{r\omega} = z_0 - \alpha_0 \\ K_{r\theta} = z_1 - \alpha_1. \end{cases} \tag{26}$$

The coefficients K_ω and K_θ are then determined by

$$\begin{bmatrix} K_\omega \\ K_\theta \end{bmatrix} = \begin{bmatrix} K_{\omega r} \\ K_{\theta r} \end{bmatrix} \begin{bmatrix} [0 \quad 1].Q_c^{-1} \\ [0 \quad 1].Q_c^{-1}.A_{mk} \end{bmatrix} \tag{27}$$

where $\boldsymbol{Q}_c$ is the controllability matrix.

The coefficients K_{θ^*} and K_L can be computed by imposing a null steady-state error and assuming a good estimation of the state variables

$$\theta^* = \hat{\theta} \text{ and } T_L = \hat{T}_L. \tag{28}$$

In steady state, the discrete model (18) becomes

$$\begin{bmatrix} \hat{\omega} \\ \hat{\theta} \end{bmatrix} = \begin{bmatrix} a_{11k} & 0 \\ a_{21k} & 1 \end{bmatrix} \begin{bmatrix} \hat{\omega} \\ \hat{\theta} \end{bmatrix} + \begin{bmatrix} b_{1k} \\ b_{2k} \end{bmatrix} I_q^* + \begin{bmatrix} e_{1k} \\ e_{2k} \end{bmatrix} T_L \tag{29}$$

$$y_m = \hat{\theta} = [0 \quad 1] \underline{\begin{bmatrix} \hat{\omega} \\ \hat{\theta} \end{bmatrix}}. \tag{30}$$

And the current reference I_q^* (19) becomes

$$I_q^* = -K_\omega \hat{\omega} - K_\theta \hat{\theta} + K_{\theta^*}\theta^* + K_L \hat{T}_L. \tag{31}$$

If we replace (30) and (31) in (29), we find the following equation

$$\hat{\theta} = K_c \left(K_{\theta^*} \begin{bmatrix} b_{1k} \\ b_{2k} \end{bmatrix} \theta^* + K_L \begin{bmatrix} b_{1k} \\ b_{2k} \end{bmatrix} \hat{T}_L + \begin{bmatrix} b_{1k} \\ b_{2k} \end{bmatrix} T_L \right) \tag{32}$$

with $K_c = [0 \quad 1] \begin{bmatrix} 1 - a_{11k} + b_{1k}K_\omega & b_{1k}K_\theta \\ -a_{21k} + b_{2k}K_\omega & b_{2k}K_\theta \end{bmatrix}^{-1}$.

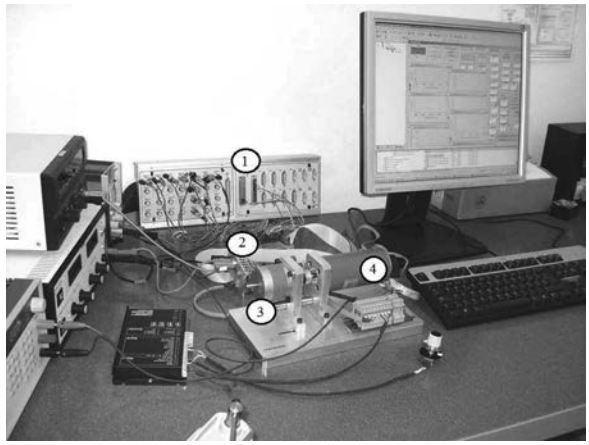

Fig. 7. Bench of test: (1) dSPACE DS1103 interface, (2) power electronics card, (3) HSM, and (4) dc Motor.

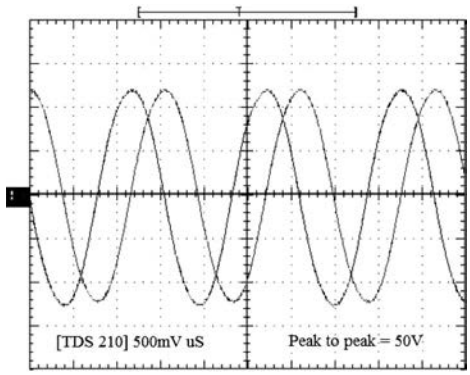

Fig. 8. Electromotive forces of the stepper motor under study.

By identification of the two sides of (32) and according to (28), we obtain the coefficients of anticipation

$$K_{\theta^*} = K_\theta \text{ and } K_L = \frac{1}{K_m}. \tag{33}$$

The experiment results (see Section V) are obtained with the following values: $\omega_0 = 200$ rad/s, $K_\omega = 0.405$, $K_\theta = K_{\theta*} = 40.746$ and $K_L = 6.536$.

IV. System Description

Fig. 7 shows the experimental bench designed to test the control developed in this paper. The various algorithms were implemented using the dSPACE DS1103 controller board based on the Motorola PowerPC 604e processor running at 933 MHz. This card also contains a DSP TM320F240 from Texas Instruments used as a slave DSP. For programming, we used MATLAB/Simulink software with the real time interface. The ControlDesk is an experimentation tool used to control, tune, and monitor the running process. We have designed a dedicated power electronic interface card. This is necessary to amplify and adapt the signal controls issued from DS1103 to the MOSFET inputs, which constitute a double H-bridge. The phase currents are measured by shunt resistances. The terminal voltages of these resistances are amplified and filtered before being applied

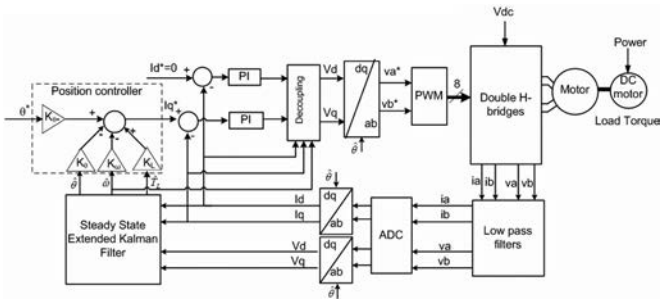

Fig. 9. Block diagram of the sensorless position control of the HSM.

to the analog-to-digital converter (ADC) inputs of the DS1103 card. In order to acquire the phase voltage, voltage dividers followed by low-pass filter were used. The choice of the pulsewidth modulation (PWM) technique is very important in order to reduce the current ripples and switching losses [26], [27]. The sinus PWM technique with a switching frequency of 10 kHz was used. In order to minimize the noises due to commutation, the ADC inputs are synchronized with the PWM signal. The ADC inputs read at the low state of PWM where the current derivative is smaller than during high state. The HSM is characterized by a 10 W power, a supply voltage of 24–60 V and a rated current of 3 A. Let us note that this is not the first time that the sensorless control techniques are applied on a motor with weak values of parameters and power. Some preceding works [3], [15], [16], [20] deal with a motor of similar values. A dc motor is coupled by a direct shaft to the HSM in order to create a load torque variation. This motor is supplied by an amplifier configured to work in a current loop control. A potentiometer is used to vary the reference current of that amplifier and then the dc motor acts as brake since the electromagnetic torque created is opposed to the torque of the HSM. In practice, the enable input of the amplifier was linked to the DS1103 card in order to control the application of step variation of the load torque by software. An incremental encoder is used only for comparison with steady-state EKF estimation. We carried out practical tests in order to confirm that the electromotive forces are sinusoidal (see Fig. 8). The block diagram of the sensorless position control is represented in Fig. 9. The steady-state EKF cannot detect the initial rotor position. To do that, a method based on the voltage impulses was used. Four successive impulse voltages were applied by using the PWM outputs of the DS1103 card. A positive impulse followed by a negative one for each phase. The initial rotor position is determined as explained in [5] by exploiting the peaks current.

V. Experimental Results

The first test checked the motor speed and position estimation by the Kalman filter. To do that, a PID position controller associated with our steady-state EKF algorithm was used. The result shown in Fig. 10(a) is obtained with a reference position of 15 rad. The initial rotor position is estimated by the impulse voltage method that we have developed and tested in [5]. When the desired position is reached ($t = 0.43$ s), the steady-state EKF cannot estimate because its inputs (current and voltage) are very weak. To solve this problem, a current of 1.5 A was injected in

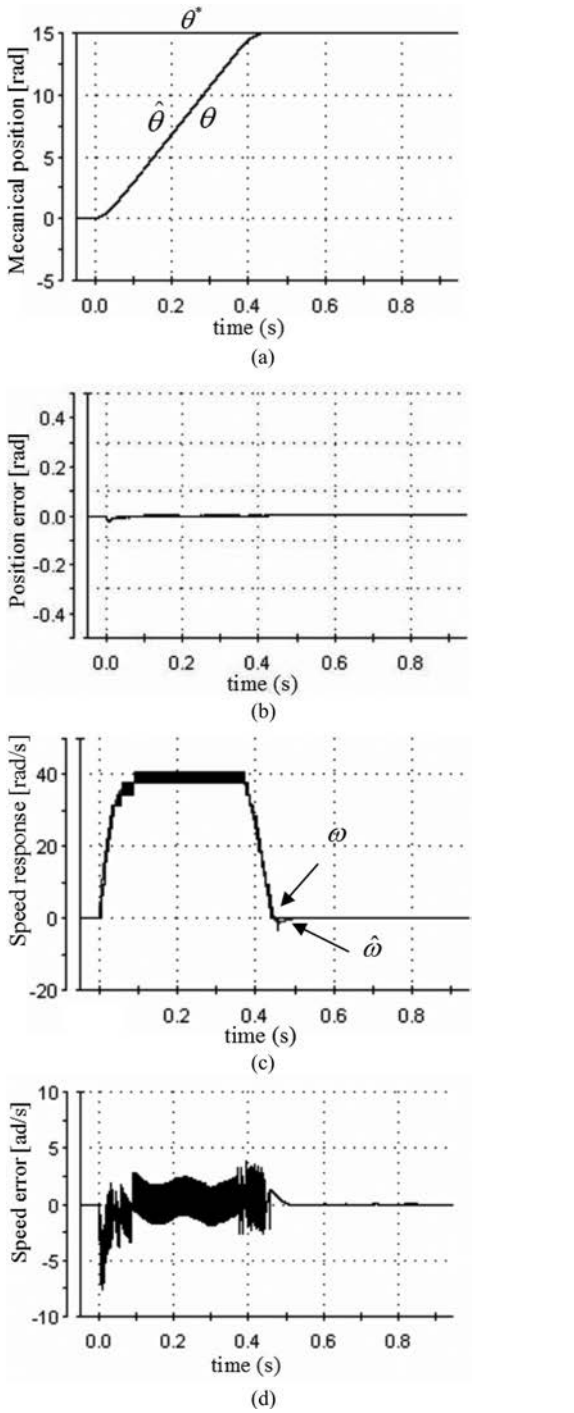

Fig. 10. Rotation of 15 rad with a PID controller. (a) Position response time. (b) Position time error ($\theta - \hat{\theta}$). (c) Estimated and measured speed. (d) Speed time error ($\omega - \hat{\omega}$).

the d-axis when the estimated position approaches its reference. In this case, the rotor can hold the position if a load torque is applied. Fig. 10(b) represents the estimated error position. We can see that in steady state this error is null. This confirms the performance of the method used for the synthesis of the steady-state EKF. Fig. 10(c) shows the speed response during the same movement. We can see that the estimated speed is very close to

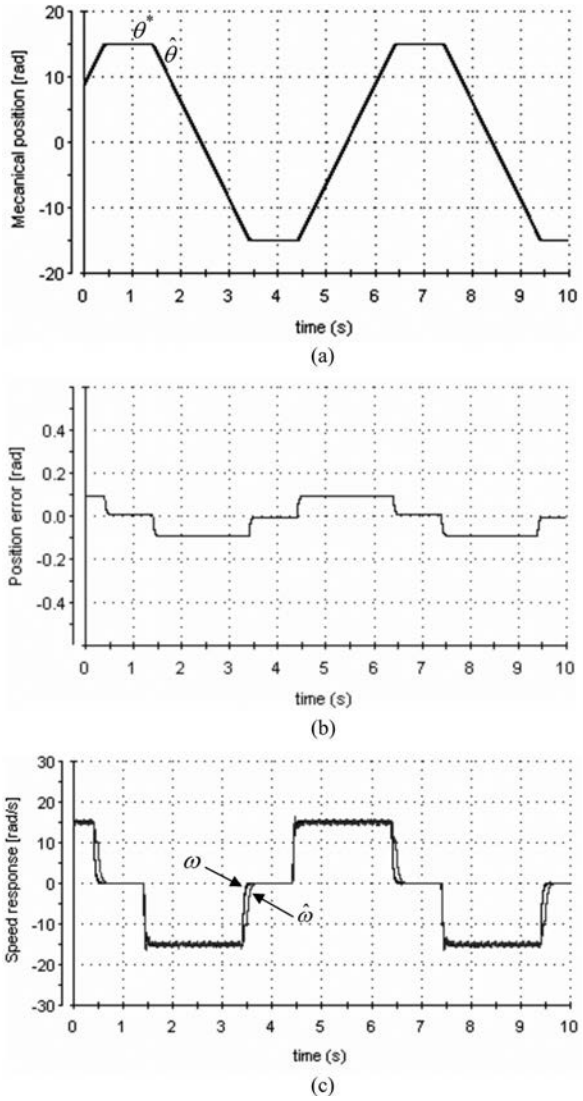

Fig. 11. Feedback control associated with the steady-state EKF. (a) Position response time. (b) Position error ($\theta^* - \hat{\theta}$). (c) Speed response time.

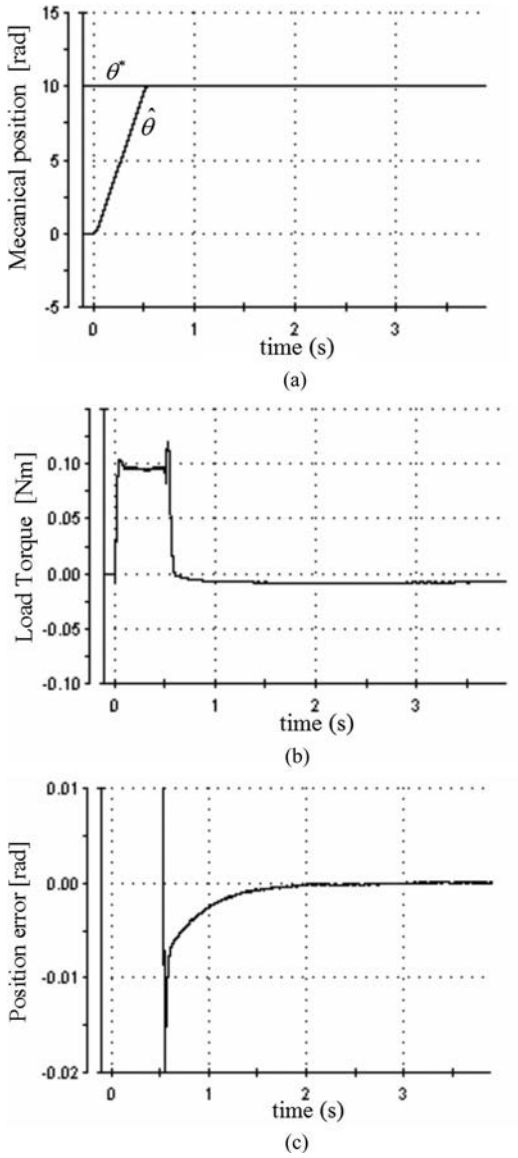

Fig. 12. Example of movement with an injected load torque. (a) Position response time. (b) Estimated load torque. (c) Position error ($\theta^* - \hat{\theta}$).

the measured one [see Fig. 10(d)]. The actual speed is affected by the pulses of the incremental encoder.

Next, the feedback controller associated with our steady-state EKF algorithm was used. A movement with a trapezoidal reference as shown in Fig. 11(a) was carried out. The error position between the reference and the estimated one is presented in Fig. 11(b). It is null in steady state and closed to a little constant value during the movement. The measured speed response and the estimated one are shown in Fig. 11(c). Compared with Fig. 10(c), the measured speed curve is filtered, here, in order to avoid the noises due to encoder impulses.

Fig. 12(a) shows an example of rotation of 10 rad with a load torque applied at startup and removed at $t = 0.5$ s. The load torque variations are created by giving a current reference value to the motor dc supply and enabling it via dSPACE software. The reference value chosen gives a load torque step of 0.1 (N·m) with very little response time as shown in Fig. 12(b). A load torque value estimated corresponds to 20% of the nominal torque. Notice that there is no mean to measure the load in the experimental benchmark. Since the feedback controller proposed here is designed with a compensation of the estimated load torque, we can see in Fig. 12(c) that the error position is null in steady state. So the position feedback control can be well achieved without a position sensor.

VI. Robustness Against Parameters Variation

Simulation tests were carried out with parameter uncertainties. The parameters are the stator resistance R, the inductance L, the motor torque constant K_m, system inertia J, and the coefficient of viscous friction K_v. The stator resistance R is the most significant parameter in the study of the robustness of the Kalman filter when applied to electrical drive. Its value can vary by $\pm 10\%$ at the ambient temperature but under several conditions it can undergo a great variation. The following variations

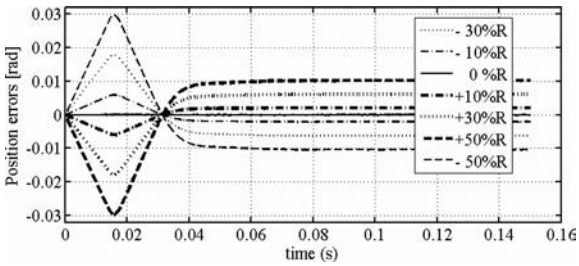

Fig. 13. Position errors $(\theta^* - \hat{\theta})$ with $-50\%R \leq \Delta R \leq +50\%R$.

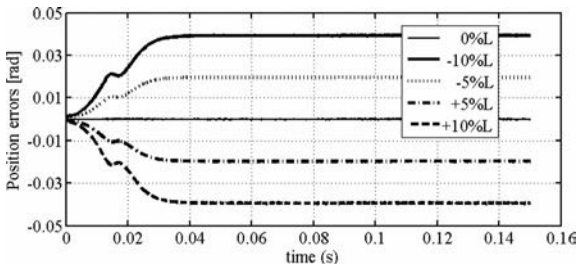

Fig. 14. Position errors $(\theta^* - \hat{\theta})$ with $-10\%L \leq \Delta L \leq +10\%L$.

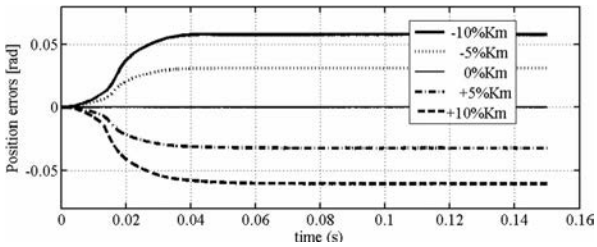

Fig. 15. Position errors $(\theta^* - \hat{\theta})$ with $-10\%K_m \leq \Delta K_m \leq +10\%K_m$.

are tested: $\pm 50\%$, $\pm 30\%$, and $\pm 10\%$. Fig. 13 represents all the estimated position errors for the various variation of the resistance R. With the ambient temperature ($\pm 10\%$ R), the position error is $\pm\ 2\ \times\ 10^{-3}$ rad. In general, the inductance L does not change. Its variation is limited to $\pm 10\%$. Fig. 14 shows that the EKF is sensitive to the variation of this parameter. For example, a weak variation of 5% on inductance leads to a position error of -0.02 rad. The motor torque constant K_m is known by the design process. As in the case of the inductance, a variation of $\pm 10\%$ was chosen. Fig. 15 shows that the variation of K_m influences in the same sense as the inductance L. Next, a variation of $\pm 10\%$ of the system inertia J is considered. In Fig. 16, we can see that the error due to the variation of this parameter is practically null. A variation of $\pm 10\%$ of the coefficient of viscous friction K_v was chosen. Fig. 17 shows that EKF is not sensitive to the variation of this parameter.

Simulation tests to verify the robustness of the proposed feedback controller against parameters variation were also carried out. The obtained results show that the variations of resistance R and inductance L have no effect on the feedback controller. This can be explained by the fact that these parameters do not appear in the controller design model (13). The variations of the motor torque constant K_m and the system inertia J have an influence only on the system time response. If K_m is increased (or

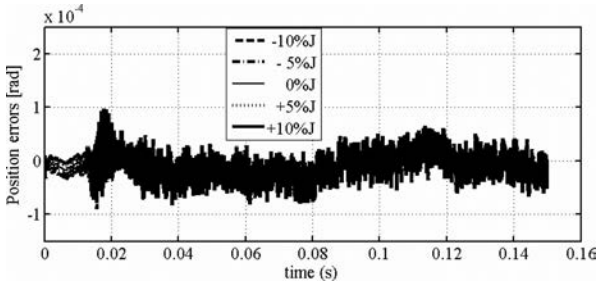

Fig. 16. Position errors $(\theta^* - \hat{\theta})$ with $-10\%J \leq \Delta J \leq +10\%J$.

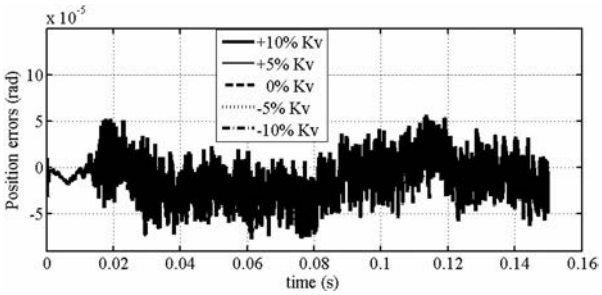

Fig. 17. Position errors $(\theta^* - \hat{\theta})$ with $-10\%K_v \leq \Delta K_v \leq +10\%K_v$.

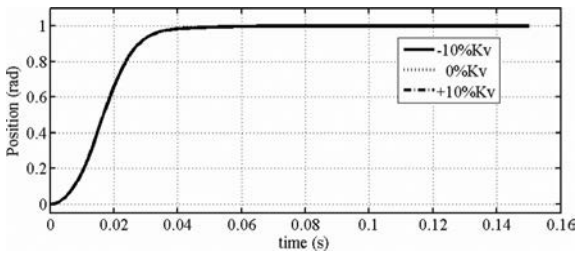

Fig. 18. Step response with $-10\%K_v \leq \Delta K_v \leq +10\%K_v$.

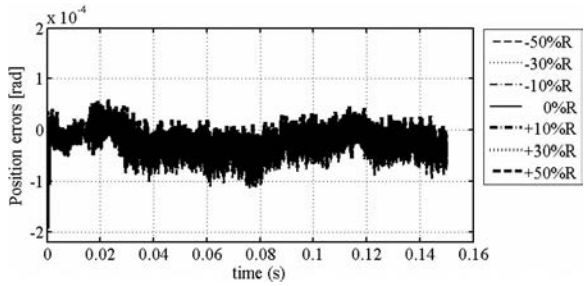

Fig. 19. Position errors $(\theta^* - \hat{\theta})$ with $-50\%R \leq \Delta R \leq +50\%R$ and resistance estimation.

J decreased), the system response becomes faster; otherwise, it becomes a little slow. Fig. 18 shows that a variation of $\pm 10\%$ of the coefficient of viscous friction K_v has no effect on feedback controller.

In regard to the all obtained simulation results shown in this section, it can be concluded that only the resistance of the motor can undergo a great variation. So, extension of the estimate of this parameter by the steady-state EKF is proposed. This can be done, as for the load torque, by including it as state variable. Considering its variation slow in regard to the sampling period,

the equation: $R_{k+1} = R_k$ is added to the system model. The result obtained, shown in Fig. 19, is very significant since the position error becomes less than 0.5×10^{-4}rad when the resistance vary between $\pm 50\%$ of its nominal value.

VII. Conclusion

In this paper, experimental results for sensorless position control of the HSM were presented. Rotor position, speed, and load torque were not measured by mechanical sensors but estimated by a steady-state EKF. Since these variables cannot be estimated at standstill, a complementary method based on the currents injection was used. The steady-state EKF is associated with a simple position feedback controller that can cancel the static error and compensate the load torque variation. In addition, the computing time of the entire system does not exceed 90 μs, which enabled a sampling period of 100 μs to be chosen. Experimental results were obtained after a good design of a dedicated electronic card was made. The good dimensioning of the current and voltage filters makes it possible to have good entries and, then, good estimates. The extension of the filter to the parameters of the system, like stator resistance *R*, improves the robustness of the proposed sensorless control. Since the computing time is reduced, implementation of the estimation of the stator resistance in real time is possible. The test bench is based on the powerful card DS1103 from dSPACE but the final objective of this paper is implementation on a DSP or FPGA.

References

[1] P. Acarnley, *Stepping Motors: A Guide to Modern Theory and Practice*, 4th ed. London, U.K.: The Institution of Engineering and Technology, 2002.

[2] Q. N. Le and J.-W. Jeon, "Neural-network-based low-speed-damping controller for stepper motor with an FPGA," *IEEE Trans. Ind. Appl.*, vol. 57, no. 9, pp. 3167–3180, Aug. 2010.

[3] Y. Anzai, S. Nishikata, and F. Tatsuta, "Studies on a sensorless initial rotor position estimating method for hybrid stepping motors," in *Proc. Int. Conf. Elect. Mach. Syst.*, Nov. 2009, pp. 1–4.

[4] M. Boussak, "Implementation and experimental investigation of sensorless speed control with initial rotor position estimation for interior permanent magnet synchronous motor drive," *IEEE Trans. Power Electron.*, vol. 20, no. 6, pp. 1413–1421, Nov. 2005.

[5] M. Bendjedia, Y. Ait-Amirat, B. Walther, and A. Berthon, "DSP implementation of rotor position detection method for hybrid stepper motors," in *Proc. Int. Power Electron. Motion Control Conf.*, 2006, vol. 3, pp. 1–3.

[6] H. Gao, F. R. Salmasi, and M. Ehsani, "Inductance model based sensorless control of the switched reluctance motor drive at low speed," *IEEE Trans. Power Electron.*, vol. 19, no. 6, pp. 1568–1573, Nov. 2004.

[7] N. Bianchi, S. Bolognani, J. Jang, and S. Sul, "Comparison of PM motor structures and sensorless control techniques for zero-speed rotor position detection," *IEEE Trans. Power Electron.*, vol. 22, no. 6, pp. 2466–2475, Nov. 2007.

[8] J. Hu, J. Liu, and L. Xu, "Eddy current effects on rotor position estimation and magnetic pole identification of PMSM at zero and low speeds," *IEEE Trans. Power Electron.*, vol. 23, no. 5, pp. 2565–2575, Sep. 2008.

[9] F. M. L. De Belie, P. Sergeant, and J. A. Melkebeek, "A sensorless drive by applying test pulses without affecting the average-current samples," *IEEE Trans. Power Electron.*, vol. 25, no. 4, pp. 875–888, Apr. 2010.

[10] H. W. De Kock, M. J. Kamper, and R. M. Kennel, "Anisotropy comparison of reluctance and PM synchronous machines for position sensorless control using HF carrier injection," *IEEE Trans. Power Electron.*, vol. 24, no. 8, pp. 1905–1913, Aug. 2009.

[11] Y. Wu, Z. Deng, X. Wang, X. Ling, and X. Cao, "Position sensorless control based on coordinate transformation for brushless DC motor drives," *IEEE Trans. Power Electron.*, vol. 25, no. 9, pp. 2365–2371, Sep. 2010.

[12] J.-B. Cao and B.-G. Cao, "Fuzzy-logic-based sliding-mode controller design for position-sensorless electric vehicle," *IEEE Trans. Power Electron.*, vol. 24, no. 10, pp. 2368–2378, Oct. 2009.

[13] Y.-S. Lai and Y.-K. Lin, "Novel back-EMF detection technique of brushless DC motor drives for wide range control without using current and position sensors," *IEEE Trans. Power Electron.*, vol. 23, no. 2, pp. 934–940, Mar. 2008.

[14] A. H. Niasar, A. Vahedi, and H. Moghbelli, "A novel position sensorless control of a four-switch, brushless DC motor drive without phase shifter," *IEEE Trans. Power Electron.*, vol. 23, no. 6, pp. 3079–3087, Dec. 2008.

[15] S. Ogasawara, "An application of sensorless drive technology to a three-phase hybrid stepping motor drive," in *Proc. Power Convers. Conf.*, Apr. 2002, pp. 964–970.

[16] S.-M. Yang and E. -Lang. Kuo, "Damping a hybrid stepping motor with estimated position and velocity," *IEEE Trans. Power Electron.*, vol. 18, no. 3, pp. 880–887, May 2003.

[17] M. S. Islam, I. Husain, R. J. Veillette, and C. Batur, "Design and performance analysis of sliding-mode observers for sensorless operation of switched reluctance motors," *IEEE Trans. Control Syst. Technol.*, vol. 11, no. 3, pp. 383–389, May 2003.

[18] G. H. B. Foo and M. F. Rahman, "Direct torque control of an IPM-synchronous motor drive at very low speed using a sliding-mode stator flux observer," *IEEE Trans. Power Electron.*, vol. 25, no. 4, pp. 933–942, Apr. 2010.

[19] J. Lee, J. Hong, K. Nam, R. Ortega, L. Praly, and A. Astolfi, "Sensorless control of surface-mount permanent-magnet synchronous motors based on a nonlinear observer," *IEEE Trans. Power Electron.*, vol. 25, no. 2, pp. 290–297, Feb. 2010.

[20] A. Ferrah, J. A.-K. Bani-Younes, M. Bouzguenda, and A. Tami, "Sensorless speed and position estimation in a stepper motor," in *Proc. Int. Aegean. Conf. Electr. Mach. Power. Electron.*, Sep. 2007, pp. 297–302.

[21] S. Bolognani, M. Zigliotto, and M. Zordan, "Extended-range PMSM sensorless speed drive based on stochastic filtering," *IEEE Trans. Power Electron.*, vol. 26, no. 1, pp. 110–117, Jan. 2001.

[22] B. Akin, U. Orguner, and A. Ersak, "A comparative study on Kalman filtering techniques designed for state estimation of industrial AC drive systems," in *Proc. Int. Conf. Mechatronics*, Jun. 2004, pp. 439–445.

[23] J. Persson and Y. Perriard, "Steady state Kalman filtering for sensorless control of hybrid stepper motors," in *Proc. IEEE Int. Conf. Elect. Mach. Drives*, Jun. 2003, vol. 2, pp. 1174–1177.

[24] P. Crnosija, B. Kuzmanovic, and S. Ajdukovic, "Microcomputer implementation of optimal algorithms for closed-loop control of hybrid stepper motor drives," *IEEE Trans. Ind. Electron.*, vol. 47, no. 6, pp. 1319–1325, Dec. 2000.

[25] S. Caux, S. Carriere, M. Fadel, and B. Sareni, "Motion control of elastic joint based on Kalman optimization with evolutionary algorithm," in *Proc. IEEE Ind. Appl. Soc. Annu. Meet. Conf.*, Oct., 2009, pp. 1–5.

[26] J. Hobraiche, J.-P. Vilain, P. Macret, and N Patin, "A new PWM strategy to reduce the inverter input current ripples," *IEEE Trans. Power Electron.*, vol. 24, no. 1, pp. 172–180, Jan. 2009.

[27] A. Iqbal and S. Moinuddin, "Comprehensive relationship between carrier-based PWM and space vector PWM in a five-phase VSI," *IEEE Trans. Power Electron.*, vol. 24, no. 10, pp. 2379–2390, Oct. 2009.